Inhibition of Copper Transport Induces Apoptosis in Triple Negative Breast Cancer Cells and Suppresses Tumor Angiogenesis

Olga Karginova*[, 1], Claire M. Weekley*[, 2], Akila Raoul[1], Alhareth Alsayed[1], Tong Wu[2], Steve Seung-Young Lee[3], Chuan He[2] and Olufunmilayo I. Olopade[1, 4]

**co-first authors*

[1]Section of Hematology/Oncology, Department of Medicine, [2]Department of Chemistry, Department of Biochemistry and Molecular Biology, Institute for Biophysical Dynamics and Howard Hughes Medical Institute, [3]Department of Molecular Genetics and Cell Biology, [4]Center for Clinical Cancer Genetics, The University of Chicago, Illinois, USA

Current address for CM Weekley: Bio21 Institute and Department of Biochemistry and Molecular Biology, The University of Melbourne, VIC, Australia

Current address for SS Lee: Department of Biopharmaceutical Sciences, College of Pharmacy, University of Illinois, Chicago, Illinois

Running Title: Targeting copper transport in breast cancer

Abbreviations: BSO, L-buthionine-sulfoximine; BSA, bovine serum albumin; CI, combination index; DRI, dose-reduction index; GSH, reduced glutathione; GSSG, oxidized glutathione; ICP-MS, inductively-coupled plasma mass spectrometry; LOX, lysyl oxidase; MAPK, mitogen-activated protein kinase; PI3K, phosphatidylinositol-3-kinase; ROS, reactive oxygen species; SOD, superoxide dismutase; TNBC, triple negative breast cancer; TM, tetrathiomolybdate; TGN, trans-Golgi network; XFM, X-ray fluorescence microscopy.

Corresponding author: Olufunmilayo I. Olopade, MD, FACP, OON
Knapp Center for Biomedical Discovery
900 E. 57th Street, 8th Floor
Chicago, Illinois 60637
Phone: 773-702-4400 * **Fax:** 773-834-0778
Email: folopade@medicine.bsd.uchicago.edu

Conflicts of Interest: C He is a scientific founder of Accent Therapeutics, Inc. and a shareholder of Epican Genentech. Other authors declare no potential conflicts of interest.

Abstract

Treatment of advanced breast cancer remains challenging. Copper and some of the copper-dependent proteins are emerging therapeutic targets as they are essential for cell proliferation and survival, and have been shown to stimulate angiogenesis and metastasis. Here we show that DCAC50, a recently developed small molecule inhibitor of the intracellular copper chaperones, ATOX1 and CCS, reduces cell proliferation and elevates oxidative stress, triggering apoptosis in a panel of triple negative breast cancer cells. Inhibition of ATOX1 activity with DCAC50 disrupts copper homeostasis, leading to increased copper levels, altered spatial copper redistribution and accumulation of ATP7B to the cellular perinuclear region. The extent and impact of this disruption to copper homeostasis varies across cell lines and correlates with cellular baseline copper and glutathione levels. Ultimately, treatment with DCAC50 attenuates tumor growth and suppresses angiogenesis in a xenograft mouse model, and prevents endothelial cell network-formation *in vitro*. Co-treatment with paclitaxel and DCAC50 enhances cytotoxicity in TNBC, and results in favorable dose reduction of both drugs. These data demonstrate that inhibition of intracellular copper transport targets tumor cells and the tumor microenvironment, and is a promising approach to treat breast cancer.

Introduction

Breast cancer is responsible for more than 250,000 new cases and 40,000 deaths among women, yearly, despite continuous efforts to improve treatment (1). Breast cancer is a biologically complex disease in its histology, molecular classification, response to therapy and mortality rates (2,3). Five intrinsic molecular subtypes (luminal A, luminal B, HER2-enriched, claudin-low, and basal-like) have been identified using comprehensive gene expression analysis of human breast cancer tissue, cell lines and mouse models (2,3). TNBC lacks estrogen and progesterone receptors, the human epidermal growth factor receptor 2, and is often associated with basal-like subtype representing a complex, clinically aggressive form of the disease (4). While 30–40% of early stage TNBC patients benefit from treatment with anthracycline and taxane-based chemotherapy, TNBC is difficult to control if it becomes resistant to treatment and spreads to distant organ sites (5-7). No specific chemotherapy agents are able to cease metastatic spread, and most TNBC patients die from advanced disease within 20 months post progression (8). A lack of molecular targets, the adaptive behavior of cancer cells and the microenvironment

contributing to tumor progression are barriers to successful therapy. To improve patient outcomes, novel treatment approaches targeting intracellular pathways and pathways involved in cross-talk between cancer cells and the tumor microenvironment are critical.

Copper and copper-dependent proteins are emerging therapeutic targets due to their involvement in cell proliferation, survival, angiogenesis and metastasis (9,10). Elevated levels of copper in blood and tumor tissue of cancer patients are correlated with disease progression (11). Copper-dependent superoxide dismutase (SOD1) is an important modulator of oxidative stress in cancer cells (12,13), and the lysyl oxidase family of proteins require copper to stabilize the extracellular matrix, which contributes to the formation of a pre-metastatic niche (14,15). Cells maintain a network of proteins (CTR1, ATP7A, ATP7B) that shuttle copper across membranes to regulate copper homeostasis to prevent damage from the redox-active metal, and deliver copper to secreted copper-dependent proteins (16). Intracellular transport of copper is mediated by chaperone proteins, ATOX1 and CCS, that supply copper to the copper-dependent ATP7A and ATP7B (Cu-ATPases), and to SOD1, respectively (17). CCS is also required for copper-mediated activation of HIF-1α to promote VEGF expression (18). ATOX1 has a possible role in metastasis: it promotes inflammatory neovascularization (19), wound closure (20) and breast cancer cell migration (21). Altogether, this evidence demonstrates that copper chaperone proteins, ATOX1 and CCS, are attractive targets for anti-cancer therapy.

Current approaches to targeting copper homeostasis include the inhibition of copper-dependent enzymes by global copper chelation, and the use of copper ionophores to elevate or redistribute copper and overwhelm the antioxidant capacity of cancer cells (22). Recently, the chelator tetrathiomolybdate (TM) was evaluated in a Phase II clinical trial for breast cancer patients with high risk of recurrence. TM suppresses angiogenesis in preclinical models (23), with its activity ascribed to the inhibition of SOD1 (13,24), LOX (25) and NF-kβ (23). TM treatment reduced serum copper levels and improved survival of breast cancer patients, including TNBC patients, demonstrating proof of principle for this approach (26). In a preclinical model, copper depletion with TM did not affect tumor growth, although it did reduce lung metastases. Despite the promising results of this trial, TM is insufficient to reduce the tumor burden in highly vascularized tumors, and may not inhibit tumor progression once an angiogenic switch has occurred (27).

An alternative approach to targeting cellular copper homeostasis is the inhibition of copper chaperones to impede copper transfer to copper-dependent enzymes and disrupt copper homeostasis. DCAC50 is a small molecule designed to inhibit intracellular copper transport by blocking the highly similar copper transfer interfaces of both ATOX1 and CCS, which prevents the protein-protein interactions necessary for copper transfer to the Cu-ATPases and SOD1, respectively (28). In leukemia and lung cancer cell lines DCAC50 reduced cell proliferation and tumor growth in xenograft mouse models without significant side effects (28).

Given the promising results of DCAC50 anti-cancer activity and the benefit of copper depletion in breast cancer patients, we studied the impact of the inhibition of copper chaperones in a broad panel of cell lines of the most aggressive breast cancer phenotype, TNBC. We describe the effects of DCAC50 on the proliferation, viability, copper homeostasis and redox status of TNBC cells. We also investigate the ability of DCAC50 to inhibit tumor growth and angiogenesis in breast cancer xenograft mouse models, and test its activity in combination with paclitaxel. This work illustrates the potential of copper transporters as targets for breast cancer treatment, shows the impact of the intracellular inhibition of copper homeostasis in TNBC, and investigates the mechanism of action.

Materials and Methods

Chemicals. DCAC50 was synthesized as previously reported (28) and was characterized by NMR and UV/Vis spectroscopy. Binding to ATOX1 was confirmed by fluorescence assay (28). DCAC50, ammonium tetrathiomolybdate (TM, 99.97%) and paclitaxel (Sigma) stocks were prepared in DMSO. L-buthionine-sulfoximine (BSO, 97%, Sigma) was prepared in water.

Cell Culture. Breast cancer cell lines were obtained from the American Type Culture Collection (Manassas, VA) and were cultured in RPMI-1640 medium supplemented with 10% FBS and antibiotic-antimycotic solution (Gibco). SUM149 cells were a gift from Dr. Perou (UNC, Chapel Hill) and were cultured in HuMEC with 5% FBS (Gibco). HMEC and HUVEC, were purchased from Lonza and cultured in MEGM or EGM-2 medium (Lonza). Cell lines were grown at 37 °C and 5 % carbon dioxide for less than 20 passages after thawing to conduct described experiments, tested negative for mycoplasma contamination and validated for species and unique DNA profile by the provider using short tandem repeat analysis. All assays were performed according to manufacturer instructions and after allowing cells to adhere overnight.

Western Blot. Cell lysates were collected in RIPA buffer (Sigma), sonicated (3 × 10 seconds) and centrifuged (10 min at 14,000 x rcf). Protein concentration was determined using Thermo Scientific™Pierce™BCA Protein Assay. Equal amount of total protein for each lysate was analyzed by SDS-PAGE and transferred to PVDF membrane (ImmobilonFL, Merk Millipore). The loading controls were from the same experimental samples. All proteins were analyzed on the same blot. The membrane was scanned using Odyssey IR Scanner. Images were analyzed using Image Studio Light (LI-COR).

Cell Proliferation. 5,000-10,000 cells were plated into a 96-well plate for each drug concentration (n = 3-6). DCAC50, TM, BSO and paclitaxel solutions were prepared as serial dilutions with total DMSO matched to vehicle control. Constant ratios of DCAC50 and paclitaxel were used when treated in combination. Solutions (2X concentrates) were added to the cells in media for 72 h at 37 °C and CellTiter 96-AQueous One Solution Assay (Promega) was performed. Data were fitted into a variable slope (four-parameter) model using GraphPad Prism. For paclitaxel and DCAC50 combination, fraction of viable cells was used to calculate combination index (CI) and dose-reduction index (DRI) using CompuSyn software (29). Alternatively, cell proliferation was assessed with The IncuCyte® S3 Live-Cell Analysis System (Essen Instruments, Ann Arbor, MI) using quantitative metrics derived after phase-contrast image acquisition, and presented as percentage of confluence.

Apoptosis. Cells were plated and treated per the proliferation assay and assayed with Caspase-Glo-3/7 assay (Promega). For the AnnexinV and propidium iodide assay, the Dead Cell Apoptosis Kit (Invitrogen) was used. Cells were plated in 6-well plates, treated, collected by trypsinization, stained and analyzed with LSR-Fortessa 4-15 (Bechton and Dickenson) instrument and FlowJo software.

Inductively-coupled plasma mass spectrometry (ICP-MS). Cells were plated in 6-well plates, treated, trypsinized, washed with PBS, collected in acid-washed tubes, digested in trace metal grade concentrated nitric acid (overnight at 37 °C, with shaking) and diluted to 2% nitric acid with ultrapure water. ^{65}Cu content was determined by ICP-MS (Agilent 7700x) with a germanium internal standard.

X-ray fluorescence microscopy (XFM). 10^6 cells/well were seeded in 6-well plates containing a silicon nitride membrane (1.5 × 1.5 mm × 500 nm, Silson, UK), serum-starved for 24 hours and full-serum media was added one hour before treatment. Cells were washed with PBS, fixed with

paraformaldehyde (3.7%, pH 7.4, 20 minutes, room temperature), washed with trace metal grade ammonium acetate (100 mM), then ultrapure water, and air-dried.

XFM was conducted at beamline 2-ID-D at the Advanced Photon Source. Samples were irradiated with a 10.1 keV beam focused through a zone plate and order-sorting aperture. X-ray fluorescence maps were generated by 'fly scanning' (1 second dwell, 0.5 μm steps). Fluorescent photons were collected by a Ge detector (UltraLEGe, Canberra) at 90° to the incident beam.

Analysis was performed using MAPS software (30) as described elsewhere (31). The nuclear region of the cell was defined as the region of high P and Zn content.

Immunofluorescence Staining and Cell Imaging. Cells were plated into 8-well glass chamber slides, coated with poly-L-lysine (Sigma), treated and fixed as for XFM microscopy, washed with PBS, permeabilized (0.1% Triton-X100 (Sigma)) and blocked with Protein Block Goat Serum (Biogenex Laboratories), stained with primary, then secondary antibodies. Cells were analyzed using Olympus IX-83 microscope controlled by Metamorph software, Olympus UPlanSAPO 40× (oil, N.A. 1.25) objective, Xcite 120 LED (Lumen Dynamics) light source, Image EMX2 CCD (Hamamatsu) camera, and ImageJ software.

ROS Assay. Cells were plated into 10 cm^2 dishes, treated, collected by trypsinization, stained with 10 μM DCFDA reagent (30 minutes, 37 °C) and washed with PBS. FACS analysis was performed using an LSR-Fortessa 4-15 (Becton and Dickenson) instrument and FlowJo software.

GSH:GSSG Assay. 20,000 cells were seeded in 96-well plates. The luminescence-based GSH/GSSG-Glo Assay (Promega) was used to determine the GSH:GSSG ratio or to calculate total GSH levels.

SOD Activity. Cells were seeded in 10 cm^2 dishes. For total SOD activity, treated cells were collected by trypsinization, washed with PBS. The cell pellet was lysed in lysis buffer (Trevigen) (30 minutes) and the supernatant was collected after centrifugation (10 minutes, 4°C, 10000 × g). Total SOD activity was determined using the SOD activity assay (Sigma). For SOD1 activity, treated cells were washed, scraped into PBS and centrifuged. The pellet was suspended in three volumes of 50 mM phosphate buffer (pH 7.6) and sonicated. Cell lysates were separated by native PAGE at 4 °C. The gel was stained as in (32) with modifications (see Supplementary Methods).

Endothelial Network-Formation. HuVEC (20,000 cells/cm^2) were plated into 48-well plates coated with phenol red-free Matrigel (Corning, 30 minutes, 37 °C), in presence of DCAC50, TM or DMSO. Cell network-formation was imaged after 16-18 h incubation at 37 °C, using an Olympus IX81 inverted microscope with the Olympus Zero Drift Correction auto re-focusing system (Olympus, USA) with a Hamamatsu Orca Flash 4.0 sCMOS camera (Hamamatsu Photonics, USA) run by Slidebook 5.0 software (Intelligent Imaging Innovations, USA), using a 10X objective with adapter and Angiogenesis Analyzer for ImageJ (NIH) (33).

LOX Assay. Cells were seeded in 24-well plates and treated in phenol red-free media. Media was collected and centrifuged to remove debris. Equal volumes of sample and reagent from Amplite Fluorimetric Lysyl Oxidase Assay Kit (AAT Bioquest) were mixed. The reactions were incubated in the dark (37 °C) and fluorescence (540 nm excitation/590 nm emission) was measured after 60 minutes.

Efficacy Study and Animal Handling. All animals were humanely handled and monitored for health conditions according to the Institutional Animal Care and Use Committee (IACUC) approved protocols. Eight-week-old female *Foxn1nu/nu* (Harlan) mice were anesthetized via inhalation with 2% vaporized isoflurane and were unilaterally injected with 4×10^6 MDA-MB-468 or 3×10^6 MDA-MB-231 cells (100 µl, 50% Matrigel) into the fourth inguinal mammary gland at the base of the nipple. 7 days post cellular implantation, animals were randomly and blindly assigned to treatment groups (6-8 per group), and treated with intraperitoneal injections of 50 mg/kg/day DCAC50 or DMSO (vehicle control). Tumor growth and weight of the animals were monitored twice weekly. Tumor measurements were performed using calipers to calculate tumor volume using formula 1/2(Length × Width^2). The assessment was blind to treatment groups and was performed by the same person throughout the study.

Immunofluorescence Staining of Tumors. Frozen tumors were thawed in RPMI-1640 media containing 10 mg/mL BSA on ice, and prepared as described previously (34). Leica TCS SP8 confocal laser scanning microscope, white light laser, Leica HCX PL APO 10X/0.4 NA dry objective (2.2 mm working distance), and a SuperZ galvometric scanning stage were used for imaging.

Results

Protein levels of copper chaperones ATOX1 and CCS are elevated in breast cancer cell lines

Elevated copper levels in serum and tissues of cancer patients (11) are a sign of altered copper homeostasis. Elevated mRNA levels of copper transport proteins have been observed in human cancers (28,35). In breast cancer tissues *ATOX1* mRNA levels were upregulated relative to normal breast tissue, but no significant change was observed for *CCS* (35). Since mRNA levels do not always correlate with protein abundance we studied the protein expression of ATOX1 and CCS in a panel of breast cancer cell lines. We included luminal and HER2-positive subtypes, as well as basal-like and claudin-low TNBC subtypes, and compared protein levels with normal human mammary epithelial cells (HMEC). Protein expression levels of ATOX1 were elevated in all breast cancer cells lines while CCS expression levels were more variable (Fig. 1A-B, Supplementary Fig. S1). The highest levels of ATOX1 were observed in luminal MCF7 (5.4-fold), claudin-low, MDA-MB-157 (6.3-fold) and basal-like MB468 (2.1-fold) cell lines. CCS protein levels were most elevated in luminal MCF7 (4.8-fold), claudin-low HCC1395 (4.1-fold) and basal-like HCC1806 (2.0-fold) cell lines. Levels of both proteins, ATOX1 and CCS, were elevated in luminal (MCF7, T47D, ZR75-1), HER-2-positive (ZR75-30), basal-like (HCC1937, HCC1806, MDA-MB-468) and claudin-low (MDA-MB-231, MDA-MB-436, HCC1395) cell lines. Since DCAC50 targets the activities of ATOX1 and CCS, we continued the study with representative cell lines of different subtypes showing variable elevated levels of these proteins.

DCAC50 reduces cell proliferation and induces apoptosis in TNBC

The cytotoxicities of the intracellular copper transport inhibitor, DCAC50, and of the copper chelator, TM, previously shown to inhibit copper-dependent enzymes in breast cancer, were evaluated using a dose-response profile in breast cancer cells. To evaluate apoptosis, we measured the activity of caspase-3/7, and estimated percentages of apoptotic cells determined by simultaneous staining with propidium iodide and AnnexinV. Treatment with DCAC50 reduced cell proliferation in a dose-dependent manner in all studied cell lines. Calculated IC50 doses varied from 5–10 μM in breast cancer cells, and higher efficacy was observed in basal-like cell lines (Fig. 1C-D). Next, we evaluated the ability of DCAC50 to induce apoptosis in the most aggressive breast cancer subtype, TNBC. Inhibition with DCAC50 resulted in activated caspase-3/7, and significantly increased percentages of apoptotic cells in all cell lines (except MDA-MB-

231), but especially in basal-like cell lines (Fig. 2A-C). Copper chelation with TM did not affect cell proliferation in studied cell lines (except for HCC1395, IC50 ~60 μM, and HCC1806, IC50 ~90 μM), and did not induce apoptosis (Fig. 2A-C, Supplementary Fig. S2A). In HMEC, no significant changes in caspase-3/7 activity were observed after treatment with DCAC50, however DCAC50 did reduce cell proliferation (IC50 = 3.5 ± 0.1 μM, Supplementary Fig. S2B-C). Thus, treatment with DCAC50 attenuates cell proliferation and leads to apoptosis-induced cancer cell death.

DCAC50 alters cellular copper homeostasis

Copper chaperone ATOX1, together with Cu-ATPases, are part of the copper export system that helps maintain copper homeostasis. While targeting copper homeostasis using chelators, such as TM, is expected to reduce cellular copper levels, the inhibition of copper transfer from ATOX1 to Cu-ATPases with DCAC50 is expected to increase cellular copper content. ICP-MS analysis revealed that overall copper content in TM-treated cells is decreased, whereas copper content in DCAC50-treated claudin-low cells is significantly increased, compared to control cells (Fig. 3A, Supplementary Fig. S3A). Surprisingly, only a modest non-significant increase in copper levels was detected in basal-like cells, which are most sensitive to DCAC50. Baseline copper levels were lower in all basal-like cells (< 9 pg Cu/μg protein) than in claudin-low cells (> 12 pg Cu/μg protein) indicating that basal-like cells may be more sensitive to marginal copper overload.

The inhibition of copper chaperones and changes in cellular copper levels are likely to lead to changes in spatial copper distribution. To better understand the impact of DCAC50 on copper homeostasis in TNBC, XFM imaging was used to determine intracellular copper distribution (Fig. 3B). In DCAC50-treated MDA-MB-231 cells, where total intracellular copper level increased with treatment, there was no significant change in the nuclear to cytoplasmic copper concentration ratio compared to control (Fig. 3B). In HCC1395 cells there was a 20% increase in the nuclear to cytoplasmic copper ratio from 1.1 to 1.3 (Supplementary Fig. S3B). In DCAC50-treated MDA-MB-468 cells, despite limited copper accumulation observed by ICP-MS, the ratio of nuclear to cytoplasmic copper concentration compared to control increased 40% from 1.2 to 1.7 (Fig. 3B). Importantly, there is no corresponding change in the localization of iron or zinc across cell lines or treatments (Supplementary Fig. S3C-D), indicating that the copper redistribution is not an artifact of sample preparation nor is it indicative of differences in cell cycle across treatment groups. Thus, inhibition of copper transport with DCAC50 alters

copper homeostasis resulting in increased copper levels and/or increased localization of copper to the nucleus. The greatest change in copper distribution with DCAC50 treatment was observed in basal-like MDA-MB-468 cells, which is the most sensitive of the three imaged cell lines to the drug.

Inhibition of ATOX1 and CCS by DCAC50 may in turn affect the level or distribution of copper transport proteins. However, the protein levels of ATP7B, ATOX1, CCS or CTR1 were unchanged after treatment with DCAC50 (Fig. S4A). The copper transporter ATP7B is known to translocate between the perinuclear space and the plasma membrane to metallate secreted copper proteins and maintain appropriate cellular copper levels (16). DCAC50 is designed to disrupt copper transfer from ATOX1 to ATP7B (28), and therefore may prevent ATP7B from translocating to the plasma membrane where it facilitates copper export. To test this hypothesis we performed immunofluorescence staining of ATP7B in MDA-MB-468 cells after treatment with DCAC50. Upon treatment, ATP7B was mostly found in the perinuclear region of MDA-MB-468 cells (Fig. 3C). In contrast, we observed diffuse staining of ATP7B in DMSO-treated cells. Thus, in basal-like MDA-MB-468 cells, DCAC50 disrupts copper homeostasis altering copper distribution and ATP7B localization.

Treatment with DCAC50 results in elevated oxidative stress

To facilitate proliferation and promote survival cancer cells frequently have to adapt to high levels of oxidative stress. Copper is intimately linked with the cellular redox status via its inherent redox activity, SOD1 activity and interactions with GSH. Thus, increased copper levels and the inhibition of copper transfer to SOD1 with DCAC50 are expected to induce oxidative stress in TNBC cells ultimately leading to cellular damage. To determine the impact of DCAC50 on cellular redox status we used a cytosolic sensor of general oxidative stress, DCFDA. Treatment with DCAC50 resulted in higher DCF fluorescence intensity generated by the oxidation of DCFDA. The fluorescence signal was higher after 24 h treatment with DCAC50 and by 72 h had increased two-fold compared to control cells (Fig. 4A-B). Copper chelation by TM had no impact on cellular oxidative stress as measured by DCF fluorescence, except for an increase observed in MDA-MB-231 cells.

Another indicator of the cellular redox environment is the oxidation state of glutathione. Lower ratios of reduced to oxidized glutathione (GSH:GSSG) were observed in all TNBC cells lines after treatment with DCAC50, indicating increased oxidative stress. Interestingly, total

GSH levels at baseline were overall higher in claudin-low cells in comparison to basal-like cells, suggesting claudin-low cells possess higher antioxidant capacity and thus, may be less sensitive to the oxidative stress triggered by DCAC50 (Fig. 4C-D, Supplementary Fig. S4B). To test if exhausting cellular antioxidant capacity by depleting GSH levels augments DCAC50's effects, we evaluated cell proliferation in claudin-low MDA-MB-436 and HCC1395 cells after treatment with DCAC50 in presence of the GSH-synthesis inhibitor, BSO. GSH levels were reduced without affecting cell proliferation after treatment with BSO, and addition of BSO to DCAC50 resulted in significantly reduced cell proliferation compared to DCAC50 alone (Fig S4C-D). This finding further supports our hypothesis that lowering cellular antioxidant capacity increases susceptibility to DCAC50.

Copper-dependent SOD1 is a known regulator of cellular redox balance, and DCAC50 has been shown to inhibit SOD1 activity in lung cancer cells, presumably by blocking copper transfer from CCS to SOD1 (28). Control experiments with TM showed reduced total SOD and SOD1 activity with copper chelation (Fig. 4E-F). However, in most TNBC cells total SOD (SOD1 and SOD2) activity increased with DCAC50 treatment after 24 h and increased further at 72 h (Fig. 4E), perhaps in response to elevated oxidative stress. Specific SOD1 activity normalized to SOD1 expression decreased in DCAC50-treated MDA-MB-231 and HCC1806 cells (Fig. 4F and Supplementary Fig. S4E-G), as expected from the inhibition of copper transfer from CCS to SOD1. However, MDA-MB-468 and HCC1395 cell lines exhibited an increase in SOD1 specific activity, which may be due to the alternative pathways for copper delivery to the enzyme (36).

The increased DCF fluorescence, lower GSH:GSSG ratio and increased total SOD activity are consistent with increased oxidative stress resulting from disruption of copper transport by DCAC50. In contrast, global copper chelation with TM has no impact on DCF fluorescence and generally reduces total SOD and SOD1 activities. Taken together, these results suggest that the general copper dyshomeostasis caused by DCAC50 is a greater contributor to the observed oxidative stress than inhibition of copper transfer from CCS to SOD1.

DCAC50 suppresses angiogenic activity of endothelial cells *in vitro*

Copper has been shown to directly stimulate angiogenesis whereas copper depletion by TM inhibits angiogenesis (23). Considering the recently reported pro-angiogenic activity of ATOX1 in endothelial cells (19), we tested if blocking ATOX1 activity with DCAC50 could suppress *in*

vitro network formation in HuVEC cells. DCAC50 reduced the number of nodes, junctions, segments and branches and the length of these elements in a network-formation assay. A smaller effect was observed for TM at the tested dose. The treatment also inhibited extracellular LOX activity, but no dose-dependent effect on cell proliferation or apoptosis was observed with DCAC50 in the HuVEC cells (Fig. 5A-C, Supplementary Fig. S5A-B). Thus, in addition to the anti-cancer effects, DCAC50 may also modulate the microenvironment by blocking angiogenesis, which may prevent vascular remodeling that is required for tumor progression.

DCAC50 inhibits tumor growth and angiogenesis in a MDA-MB-468 xenograft model

Taking into account the promising anti-cancer activity of DCAC50 *in vitro*, we evaluated the efficacy of copper transport inhibition in xenograft mouse models. In MDA-MB-468 xenografts, treatment with DCAC50 resulted in the inhibition of tumor growth and reduced tumor volumes, in comparison to the control (vehicle) group of mice (Fig. 5D, Supplementary Fig. S6A). Importantly, in addition to the inhibition of tumor growth in MDA-MB-468 xenografts, we observed significantly suppressed angiogenesis, as indicated by the reduced blood vessel area in DCAC50-treated mice, detected by staining with $CD31^+$ and $CD105^+$, vascular and neovascular endothelial cell markers, respectively (Fig. 5E-G). Reduced angiogenesis was also observed in MDA-MB-231 xenografts; although tumor volumes did not change overall at the end of treatment, slower tumor growth in 3 of 8 mice was observed (Supplementary Fig. S6B-D). The lower sensitivity of the MDA-MB-231 model to DCAC50 treatment is in concordance with our data observed *in vitro*. Thus, inhibition of intracellular copper transport by DCAC50 can suppress tumorigenesis by targeting both tumor cells and the tumor microenvironment, but its anti-tumor activity varies due to different sensitivities of TNBC cells to the disruption of copper homeostasis.

Inhibition of copper transport with DCAC50 in combination with paclitaxel induces synergistic cytotoxicity

Treatment of patients with TNBC relies heavily on chemotherapy including anthracyclines, taxanes, platinum agents and their combinations. The combination of chemotherapy with targeted therapy may result in fewer adverse effects and improve therapeutic efficacy, particularly in advanced cases. To explore this concept we evaluated the benefits of DCAC50 treatment in combination with paclitaxel. We conducted multi-drug combination dose–response analysis in TNBC cells using the Chou-Talalay method (29) (Fig. 6A). Co-treatment of

paclitaxel and DCAC50 resulted in a CI less than one, suggesting additive to synergistic cytotoxicity (Fig. 6B). In addition, we observed a favorable dose reduction for both drugs, when cell lines were treated with the above combination, as indicated by DRI values ranging from 1.60-3.45 for DCAC50 and 2.04-3.72 for paclitaxel. While the efficacy of the treatment combination leads to the additive cytotoxicity in MDA-MB-231, MDA-MB-436, MDA-MB-468 and HCC1395 cell lines (CI ranging from 0.9 to 1.1), we observed a synergistic response in HCC1187 and HCC1806 cell lines (CI < 0.9). Since the cytotoxicity of DCAC50 in tumor cells is a consequence of elevated oxidative stress, we hypothesized that the greater cytotoxicity of the co-treatment could be explained by increased oxidative stress, compared to paclitaxel alone. Co-treatment of paclitaxel and DCAC50 resulted in significantly higher oxidative stress in all examined cancer cell lines, in comparison to paclitaxel alone (Fig. 6C). Oxidative stress in paclitaxel-treated cells is reduced, compared to DMSO-treated cells. Thus, combination of DCAC50 with paclitaxel increases oxidative stress in tumor cells resulting in greater cytotoxicity.

Discussion

In breast cancer, elevated levels of copper and copper-related proteins are associated with advanced disease (37-39), remodeling of the tumor microenvironment (14,26) and resistance to chemotherapy (39,40). Thus, copper homeostasis and the copper proteome are targets for breast cancer therapy. We have investigated an emerging approach to targeting copper-dependent cellular functions via the inhibition of intracellular copper transport in TNBC using the novel small molecule DCAC50. We demonstrate that DCAC50 reduces cell proliferation and induces apoptosis through the inhibition of copper transport, disruption of cellular copper homeostasis, and the generation of oxidative stress in a panel of TNBC cell lines. Furthermore, DCAC50 enhances the cytotoxicity of paclitaxel in vitro, and inhibits tumor growth and angiogenesis in a xenograft mouse model.

The inhibition of ATOX1 and CCS activity with DCAC50 is expected to disrupt copper homeostasis and the copper proteome. In our study, significant increases in total intracellular copper levels were observed with DCAC50 treatment in claudin-low cells and modest increases in basal-like cells. Copper distribution was changed, with copper accumulating in the nuclei in MDA-MB-468 cells, to a lesser extent in HCC1395 nuclei or not at all in MDA-MB-231 nuclei.

Attenuated cell proliferation and induced apoptosis were observed in all DCAC50-treated cell lines. Thus, the alteration of copper homeostasis, observed as an increase in total copper content and/or changes in copper distribution, leads to cytotoxicity. Nuclear localization of copper has previously been reported in in *Atox1*$^{-/-}$ mouse embryonic fibroblasts (41), in ATP7A-deficient skin fibroblasts (42) and in *Atp7b*$^{-/-}$ mouse hepatocytes (43). However, the consequences of nuclear copper localization on cell proliferation, and the question of how copper enters the nuclei when the copper transport pathway is perturbed, remain to be elucidated. ATOX1 has been identified as a nuclear transcription factor and may undergo copper-dependent translocation to the nucleus (44). However, ATOX1 distributions were unchanged in DCAC50-treated cells (Figure S4A).

Various copper transporters regulate cellular copper content and its distribution. Cu-ATPases – downstream targets of ATOX1 – translocate between the perinuclear space associated with TGN, where they supply copper to cuproenzymes, and the plasma membrane, to export copper from the cell (16). Copper binding is necessary for Cu-ATPase re-localization, and Cu-ATPase mutants unable to bind copper are restricted to the TGN (45). Thus, the inhibition of copper transfer from ATOX1 is expected to alter the distribution of Cu-ATPases. In MDA-MB-468 cells, DCAC50 changed the localization of ATP7B resulting in enhanced ATP7B clustering near the nuclei, which is indicative of impaired copper homeostasis. However, DCAC50 did not induce noticeable changes in protein levels of ATP7B, ATOX1, CTR1 or CCS, indicating no effect of the treatment on protein synthesis or degradation. In summary, DCAC50 causes changes in ATP7B and copper localization, but the detailed mechanism by which copper is translocated to the nucleus and how this impacts cell proliferation and survival remains unclear.

Copper homeostasis and copper-dependent proteins are intimately linked with the redox status of cells. Intracellular copper homeostasis is tightly regulated to protect cells from exposure to the redox-active metal. Free copper can induce superoxide generation and bind glutathione to create an oxidizing environment. On the other hand, copper-dependent SOD1 and total SOD (SOD1 and SOD2) activities are responsive to superoxide levels and protect cells from excessive oxidative stress. ATOX1 itself has a central role linking copper and redox homeostasis (46). Therefore, disruption of copper homeostasis and the copper proteome is expected to disrupt cellular redox status. We have observed increased oxidative stress in all DCAC50-treated cells, measured by general ROS levels and the change in the GSH:GSSG ratio. Overall, oxidative stress precedes the induction of apoptosis in cancer cells, suggesting that elevation of ROS is the

reason for cytotoxicity. Inhibition of intracellular copper transport by DCAC50 is expected to inhibit the activity of copper-dependent SOD1. In our study, total SOD activity increased over time with increasing ROS levels, presumably in an effort to modulate oxidative stress. At the same time, SOD1 activity, normalized to SOD1 expression, decreased with DCAC50 treatment in some cell lines, as expected with the inhibition of copper transfer from CCS to SOD1, but increased in others. SOD1 has a half-life of more than 30 hours in mammalian cells (47) and alternative pathways exist for the delivery of copper to the enzyme (36), which may mitigate the impact of DCAC50 on SOD1 activity.

ATOX1 and CCS protein expression levels and IC50 values for DCAC50 were established in eight breast cancer cell lines and in normal mammary epithelial cells (HMEC). Low micromolar IC50s were obtained in all cell lines, with no clear correlation between copper chaperone protein levels and sensitivity to DCAC50. Ultimately, six TNBC cell lines with variable elevated levels of ATOX1 and CCS were selected to investigate the effects of copper transport inhibition. We found that DCAC50 inhibited proliferation and induced apoptosis more effectively in basal-like than in claudin-low cell lines. To explain the broadly different responses of these subtypes of cells to DCAC50, we must consider cellular copper and redox statuses. High copper levels at baseline and large increases in intracellular copper levels with treatment were observed in claudin-low cells (MDA-MB-231, MDA-MB-436, HCC1395), yet DCAC50 was less effective in these cells lines. Basal-like MDA-MB-468 cells, which had lower baseline copper levels that increased only modestly with treatment, exhibited noticeable disruption to copper distribution and were particularly sensitive to DCAC50-induced apoptosis. Denoyer *et al*. have argued that the sensitivity of cancer cells to ROS-generating copper ionophores may be attributed to limited antioxidant capacity rather than to high basal copper levels (48). Our data indicate that the ability of breast cancer cells to control ROS production is an important contributor to sensitivity to DCAC50. One of the major cellular antioxidant molecules, glutathione, binds copper and has been shown to protect cells from ROS toxicity (49,50). In mouse embryonic fibroblasts, when glutathione levels are low, ATOX1 deficiency has been shown to disrupt copper homeostasis leading to cell death (51). This evidence suggests that when glutathione levels are low and ATOX1 is limited, cells are susceptible to copper dyshomeostasis and oxidative stress. In our study, basal-like cells (MDA-MB-468, HCC1187, HCC1806) had overall lower copper levels and lower total GSH levels at baseline, in comparison to claudin-low cells. Thus, basal-like cells may have a lower threshold for copper overload, and may be more

sensitive to copper dyshomeostasis and oxidative stress when ATOX1 is inhibited by DCAC50. In contrast, claudin-low cells possess higher levels of glutathione and resist oxidative stress caused by DCAC50 treatment. Our results demonstrate that the GSH synthesis inhibitor, BSO, potentiates DCAC50 inhibition of cell proliferation in claudin-low HCC1395 and MDA-MB-436 cells by depleting glutathione levels and thus exhausting cellular antioxidant defense.

Of all the TNBC cell lines evaluated in this study, MDA-MB-231 cells are most resistant to DCAC50's cytotoxic effects, which may be a consequence of distinct genetic alterations promoting cell growth and survival. MDA-MB-231 cell line is an invasive, highly metastatic claudin-low cell line that bears activating mutations in KRAS, BRAF and PDGFRa, which have previously been shown to upregulate cell proliferation and survival through activation of MAPK and PI3K (52,53). Moreover, MDA-MB-231 cells can upregulate the anti-apoptotic gene BCL2A1 upon tumor progression (54). Thus, activation of these alternative signaling pathways may contribute to the ability of MDA-MB-231 cells to resist DCAC50 treatment. In comparison to cancer cells, the disruption of copper homeostasis with DCAC50 triggered a limited response in normal cells (HMEC and HuVEC). DCAC50 attenuated cell proliferation in HMEC and inhibited network-formation in HuVEC (without reducing cell proliferation), but no induction of apoptosis was detected in either of the normal cell lines. DCAC50 has previously been shown to have a minimal effect on the proliferation of other normal human cell lines (28). The ability of cells to activate pathways to resist copper toxicity and oxidative stress, may explain heterogeneous sensitivity to DCAC50 and to the associated copper overload.

Reactive oxygen species are relevant to paclitaxel cytotoxicity, and resistance to paclitaxel relies, at least partially, on cellular total antioxidant capacity (55). Co-treatment with DCAC50 elevates oxidative stress, and is expected to enhance cytotoxicity in paclitaxel-treated cells. We observed increased production of oxidative stress and improved efficacy in cells treated by paclitaxel in combination with DCAC50, in comparison to paclitaxel alone. We hypothesize that the efficacy of the combination is due to the interference of multiple pathways involved in the defense against oxidative stress. The combination was effective to reduce treatment doses for both drugs, and may help reduce paclitaxel-associated side effects and reverse paclitaxel-associated resistance in tumor cells.

The findings presented here support our hypothesis that DCAC50 inhibits copper transport and alters copper homeostasis, disrupting the redox balance and causing cytotoxicity in

cancer cells. The varying efficacy of DCAC50 reflects the heterogeneity of breast cancer cell lines and suggests that the success of drugs targeting copper homeostasis may depend on baseline cellular copper and redox statuses. Our findings also reveal the differences between targeting copper homeostasis, via the intracellular copper transport pathway, versus global copper chelation. Recent studies suggest that copper chelation is clinically important, especially for high-risk breast cancer patients and in the prevention of angiogenesis and metastasis. In our study, TM did not have a significant effect on cancer cell growth or survival, however it did inhibit endothelial cell network-formation *in vitro*, in accordance with its known antiangiogenic activity (23). Importantly, DCAC50 targets tumor cell viability as well as the tumor microenvironment, thus the inhibition of intracellular copper transport has the potential to become an effective strategy to treat breast cancer.

We conclude that dual effects of triggering apoptosis in tumor cells and modulating the tumor vascular environment are extremely attractive and should prompt further evaluation of the copper transport pathway as a therapeutic target in breast cancer.

Acknowledgements

Use of the Advanced Photon Source at Argonne National Laboratory was supported by the US Department of Energy, Office of Science, and Office of Basic Energy Sciences, under contract DE-AC02-06CH11357. We thank the US Department of Energy, under contract number DE-FG02-07ER15865 to C He for partial support of this work. We acknowledge funding from Breast Cancer Research Foundation FP049439 (OI Olopade), the National Health and Medical Research Council (Australia) to CM Weekley (CJ Martin Overseas Biomedical Fellowship APP1090612) and NIBIB K99 EB022636 to SS Lee. We thank Dr. Andrei Karginov for helpful comments and assistance with cell imaging, and Dr. Barry Lai for his assistance with XFM imaging.

References

1. Howlander N. SEER Cancer Statistics Review, 1975-2014. Howlander N, Noone A, Krapcho M, Miller D, Bishop K, Kosary C, et al., editors. Bethseda, MD. Available from: https://seer.cancer.gov/csr/1975_2014/

2. Prat A, Perou CM. Deconstructing the molecular portraits of breast cancer. Mol Oncol. 2011;5:5–23.

3. Prat A, Adamo B, Cheang MCU, Anders CK, Carey LA, Perou CM. Molecular characterization of basal-like and non-basal-like triple-negative breast cancer. The Oncologist. 2013;18:123–33.

4. Carey L, Winer E, Viale G, Cameron D, Gianni L. Triple-negative breast cancer: disease entity or title of convenience? Nat Rev Clin Oncol. 2010;7:683–92.

5. Cortazar P, Zhang L, Untch M, Mehta K, Costantino JP. Pathological complete response and long-term clinical benefit in breast cancer: the CTNeoBC pooled analysis. The Lancet. 2014;384:164–72.

6. Liedtke C, Mazouni C, Hess KR, André F, Tordai A, Mejia JA, et al. Response to Neoadjuvant Therapy and Long-Term Survival in Patients With Triple-Negative Breast Cancer. J Clin Oncol. 2008;26:1275–81.

7. Carey LA, Dees EC, Sawyer L, Gatti L, Moore DT, Collichio F, et al. The Triple Negative Paradox: Primary Tumor Chemosensitivity of Breast Cancer Subtypes. Clin Cancer Res. 2007;13:2329–34.

8. Bonotto M, Gerratana L, Poletto E, Driol P, Giangreco M, Russo S, et al. Measures of outcome in metastatic breast cancer: insights from a real-world scenario. The Oncologist. 2014;19:608–15.

9. Denoyer D, Masaldan S, La Fontaine S, Cater MA. Targeting copper in cancer therapy: 'Copper That Cancer'. Metallomics. 2015;7:1459–76.

10. Ackerman CM, Chang CJ. Copper signaling in the brain and beyond. J Biol Chem. 2018;293:4628–35.

11. Gupte A, Mumper RJ. Elevated copper and oxidative stress in cancer cells as a target for cancer treatment. Cancer Treat Rev. 2009;35:32–46.

12. Papa L, Hahn M, Marsh EL, Evans BS, Germain D. SOD2 to SOD1 Switch in Breast Cancer. 2014;289:5412–6.

13. Glasauer A, Sena LA, Diebold LP, Mazar AP, Chandel NS. Targeting SOD1 reduces experimental non–small-cell lung cancer. J Clin Invest. 2013;124:117–28.

14. Erler JT, Bennewith KL, Nicolau M, Dornhöfer N, Kong C, Le Q-T, et al. Lysyl oxidase is essential for hypoxia-induced metastasis. Nature. 2006;440:1222–6.

15. Wiel C, Augert A, Vincent DF, Gitenay D, Vindrieux D, Le Calv eacute B, et al. Lysyl oxidase activity regulates oncogenic stress response and tumorigenesis. Cell Death Dis. 2013;4:e855.

16. Gupta A, Lutsenko S. Human copper transporters: mechanism, role in human diseases and therapeutic potential. Future Med Chem. 2009;1:1125–42.

17. Huffman DL, O'Halloran TV. Function, structure, and mechanism of intracellular copper trafficking proteins. Annu Rev Biochem. 2001;70:677–701.

18. Feng W, Ye F, Xue W, Zhou Z, Kang YJ. Copper regulation of hypoxia-inducible factor-1 activity. Mol Pharmacol. 2009;75:174–82.

19. Chen G-F, Sudhahar V, Youn S-W, Das A, Cho J, Kamiya T, et al. Copper Transport Protein Antioxidant-1 Promotes Inflammatory Neovascularization via Chaperone and Transcription Factor Function. Sci Rep. 2015;5:14780.

20. Das A, Sudhahar V, Chen G-F, Kim HW, Youn S-W, Finney LA, et al. Endothelial Antioxidant-1: a Key Mediator of Copper-dependent Wound Healing in vivo. Sci Rep. 2016;6:33783.

21. Blockhuys S, Wittung-Stafshede P. Copper chaperone Atox1 plays role in breast cancer cell migration. Biochem Biophys Res Commun. 2017;483:301–4.

22. Weekley CM, He C. Developing drugs targeting transition metal homeostasis. Curr Opin Chem Biol. 2017;37:26–32.

23. Pan Q, Kleer CG, van Golen KL, Irani J, Bottema KM, Bias C, et al. Copper deficiency induced by tetrathiomolybdate suppresses tumor growth and angiogenesis. Cancer Res. 2002;62:4854–9.

24. Juarez JC, Betancourt O, Pirie-Shepherd SR, Guan X, Price ML, Shaw DE, et al. Copper binding by tetrathiomolybdate attenuates angiogenesis and tumor cell proliferation through the inhibition of superoxide dismutase 1. Clin Cancer Res. 2006;12:4974–82.

25. Kumar P, Yadav A, Patel SN, Islam M, Pan Q, Merajver SD, et al. Tetrathiomolybdate inhibits head and neck cancer metastasis by decreasing tumor cell motility, invasiveness and by promoting tumor cell anoikis. Mol Cancer. 2010;9:206.

26. Chan N, Willis A, Kornhauser N, Ward MM, Lee SB, Nackos E, et al. Influencing the Tumor Microenvironment: A Phase II Study of Copper Depletion Using Tetrathiomolybdate in Patients with Breast Cancer at High Risk for Recurrence and in Preclinical Models of Lung Metastases. Clin Cancer Res. 2017;23:666–76.

27. Crowe A, Jackaman C, Beddoes KM, Ricciardo B, Nelson DJ. Rapid copper acquisition by developing murine mesothelioma: decreasing bioavailable copper slows tumor growth, normalizes vessels and promotes T cell infiltration. PLoS ONE. 2013;8:e73684.

28. Wang J, Luo C, Shan C, You Q, Lu J, Elf S, et al. Inhibition of human copper trafficking by a small molecule significantly attenuates cancer cell proliferation. Nat Chem. 2015;7:968–79.

29. Chou TC. Drug Combination Studies and Their Synergy Quantification Using the Chou-Talalay Method. Cancer Res. 2010;70:440–6.

30. Vogt S. MAPS: A set of software tools for analysis and visualization of 3D X-ray fluorescence data sets. J Phys IV. 2003;104:635–8.

31. Weekley CM, Kenkel I, Lippert R, Wei S, Lieb D, Cranwell T, et al. Cellular Fates of Manganese(II) Pentaazamacrocyclic Superoxide Dismutase (SOD) Mimetics: Fluorescently Labeled MnSOD Mimetics, X-ray Absorption Spectroscopy, and X-ray Fluorescence Microscopy Studies. Inorg Chem. 2017;56:6076–93.

32. Chen CN, Pan SM. Assay of superoxide dismutase activity by combining electrophoresis and densitometry. Bot Bull Acad Sin. 1996;37:107–11.

33. Lee E, Lee SJ, Koskimaki JE, Han Z, Pandey NB, Popel AS. Inhibition of breast cancer growth and metastasis by a biomimetic peptide. Sci Rep. 2014;4:52–12.

34. Lee SS-Y, Bindokas VP, Kron SJ. Multiplex three-dimensional optical mapping of tumor immune microenvironment. Sci Rep. 2017;7:17031.

35. Blockhuys S, Celauro E, Hildesjö C, Feizi A, Stål O, Fierro-González JC, et al. Defining the human copper proteome and analysis of its expression variation in cancers. Metallomics. 2017;9:112–23.

36. Carroll MC, Girouard JB, Ulloa JL, Subramaniam JR, Wong PC, Valentine JS, et al. Mechanisms for activating Cu- and Zn-containing superoxide dismutase in the absence of the CCS Cu chaperone. Proc Natl Acad Sci USA. 2004;101:5964–9.

37. Choong LY, Lim S, Chong PK, Wong CY, Shah N, Lim YP. Proteome-Wide Profiling of the MCF10AT Breast Cancer Progression Model. Aziz SA, editor. PLoS ONE. 2010;5:e11030–8.

38. Kuo HW, Chen SF, Wu CC, Chen DR, Lee JH. Serum and tissue trace elements in patients with breast cancer in Taiwan. Biol Trace Elem Res. 2002;89:1–11.

39. Kanzaki A, Toi M, Neamati N, Miyashita H, Oubu M, Nakayama K, et al. Copper-transporting P-type adenosine triphosphatase (ATP7B) is expressed in human breast carcinoma. Jpn J Cancer Res. 2002;93:70–7.

40. Chisholm CL, Wang H, Wong AH-H, Vazquez-Ortiz G, Chen W, Xu X, et al. Ammonium tetrathiomolybdate treatment targets the copper transporter ATP7A and enhances sensitivity of breast cancer to cisplatin. Oncotarget. 2016;7:84439–52.

41. McRae R, Lai B, Fahrni CJ. Copper redistribution in Atox1-deficient mouse fibroblast cells. J Biol Inorg Chem. 2009;15:99–105.

42. Bhattacharjee A, Yang H, Duffy M, Robinson E, Conrad-Antoville A, Lu Y-W, et al. The Activity of Menkes Disease Protein ATP7A Is Essential for Redox Balance in Mitochondria. J Biol Chem. 2016;291:16644–58.

43. Ralle M, Huster D, Vogt S, Schirrmeister W, Burkhead JL, Capps TR, et al. Wilson disease at a single cell level: intracellular copper trafficking activates compartment-specific responses in hepatocytes. J Biol Chem. 2010;285:30875–83.

44. Itoh S, Kim HW, Nakagawa O, Ozumi K, Lessner SM, Aoki H, et al. Copper chaperone Atox1 interacts with the metal-binding domain of Wilson's disease protein in cisplatin detoxification. J Biol Chem. 2008;283:9157–67.

45. Strausak D, La Fontaine S, Hill J, Firth SD, Lockhart PJ, Mercer JF. The role of GMXCXXC metal binding sites in the copper-induced redistribution of the Menkes protein. J Biol Chem. 1999;274:11170–7.

46. Hatori Y, Lutsenko S. The Role of Copper Chaperone Atox1 in Coupling Redox Homeostasis to Intracellular Copper Distribution. Antioxidants. 2016;5:25–16.

47. Bartnikas TB, Gitlin JD. Mechanisms of biosynthesis of mammalian copper/zinc superoxide dismutase. J Biol Chem. 2003;278:33602–8.

48. Denoyer D, Pearson HB, Clatworthy SAS, Smith ZM, Francis PS, Llanos RM, et al. Copper as a target for prostate cancer therapeutics: copper-ionophore pharmacology and altering systemic copper distribution. Oncotarget. 2016;7:37064–80.

49. Kalinina EV, Chernov NN, Novichkova MD. Role of glutathione, glutathione transferase, and glutaredoxin in regulation of redox-dependent processes. Biochemistry Moscow. 2015;79:1562–83.

50. Freedman JH, Ciriolo MR, Peisach J. The role of glutathione in copper metabolism and toxicity. J Biol Chem. 1989;264:5598–605.

51. Hatori Y, Clasen S, Hasan NM, Barry AN, Lutsenko S. Functional partnership of the copper export machinery and glutathione balance in human cells. J Biol Chem. 2012;287:26678–87.

52. Van Stry M, Kazlauskas A, Schreiber SL, Symes K. Distinct effectors of platelet-derived growth factor receptor-alpha signaling are required for cell survival during embryogenesis. Proc Natl Acad Sci USA. 2005;102:8233–8.

53. Leiser D, Medová M, Mikami K, Nisa L, Stroka D, Blaukat A, et al. KRAS and HRAS mutations confer resistance to MET targeting in preclinical models of MET-expressing tumor cells. Mol Oncol. 2015;9:1434–46.

54. Kim M-Y, Oskarsson T, Acharyya S, Nguyen DX, Zhang XHF, Norton L, et al. Tumor Self-Seeding by Circulating Cancer Cells. Cell. 2009;139:1315–26.

55. Ramanathan B, Jan K-Y, Chen C-H, Hour T-C, Yu H-J, Pu Y-S. Resistance to Paclitaxel Is Proportional to Cellular Total Antioxidant Capacity. Cancer Res. 2005;65:8455–60.

Figures Legends

Figure 1. A-B. Protein levels of ATOX1 and CCS in breast cancer cell lines in comparison to normal cells (HMEC). Relative protein expression is presented as mean ± SD in breast cancer cells compared to normal cells (HMEC) and was determined using at least two biological and two technical replicates (see Supplementary Figure S1 for representatives of full blots). Equal amount of total protein was loaded for each sample. **C.** Representative dose-response profiles of DCAC50 in breast cancer cell lines. Fraction of viable cells was determined using after treatment with escalating doses of DCAC50 (see Cell Proliferation Assay). Data were fitted into variable slope (four-parameter) model using GraphPadPrism to estimate IC50. **D.** Efficacy and potency of DCAC50. IC50 dose and maximum percentage of affected cells were calculated from at least three independent experiments. Data are presented as mean ± SD.

Figure 2. Effect of DCAC50 and tetrathiomolybdate (TM) on apoptosis in TNBC cells lines. **A**. TNBC cells stained with Annexin V (AnV) and propidium iodide (PI). Percent of apoptotic cells was calculated as the sum of early apoptotic (AnV+/PI-) and late apoptotic (AnV+/PI+) cells. Cells were treated for 72 h with 20 μM DCAC50, 30 μM TM or 20 μM cisplatin, stained and analyzed by flow cytometry. Mean ± SD of three biological replicates are reported. *P < 0.05, versus DMSO control, according to two-tailed Student's *t*-test. **B**. Flow cytometry analysis of HCC1806 cells treated with DCAC50 (upper panel) or DMSO (lower panel) in a representative experiment. **C**. Caspase-3/7 activity assay. Percent change of relative luminescence signal normalized to viability obtained from a simultaneous proliferation assay and proportional to caspase-3/7 activity after 72 h treatment with 20 μM DCAC50 in comparison to DMSO. Mean ± SD of two biological with three technical replicates are reported. *P < 0.05, versus DMSO control, according to two-tailed Student's *t*-test.

Figure 3. Cellular copper content and distributions of copper and ATP7B in treated cells. **A.** Copper content was determined by ICP-MS of bulk cell pellets after treatment with DMSO, 20 μM DCAC50 or 30 μM TM for 24 h and was normalized to protein concentration. Outliers identified by the Grubbs' test were removed. Mean ± SD of four to six biological replicates. *P < 0.05, compared to DMSO control, according to two-tailed Student's t-test. **B.** Distribution of copper (nuclear vs. cytosolic) in cells treated with DCAC50. The ratio of cytoplasmic to nuclear Cu concentration (top) in MDA-MB-B231 and MDA-MB-468 cells treated with DMSO or 20 μM DCAC50 for 24 hours. Visible light microscope images and XFM elemental maps (bottom) of P, Fe, Cu and Zn are shown for representative cells within each sample, matched to the corresponding data points in the graphs by a square or star. Mean ± SD for n = 9-10 cells. *P < 0.05, compared to DMSO control, according to two-tailed Student's t-test; ns, not significant. A 10 μm scale bar is included in each Zn map and the relative elemental concentration within each cell is indicated by the intensity scale. **C.** Representative fluorescent images of MDA-MB-468 cells treated with DMSO or 20 μM DCAC50 for 24 h and stained with DAPI and antibodies against ATP7B. Arrows indicate accumulation of ATP7B in the perinuclear region of cells. Scale bar = 10 μm.

Figure 4. Effect of DCAC50 on levels of oxidative stress. A-B. DCF fluorescence in cells treated with DCAC50 or TM. TNBC cells were treated with DMSO, 20 μM DCAC50 or 30 μM TM and stained with DCFDA. Data are presented as (A) fold-change in DCF fluorescence intensity (mean ± SD of at least two biological replicates) and (B) representative histogram of the flow cytometry analysis of MDA-MB-468 cells. **C**. The oxidation state of glutathione after treatment with DCAC50. GSH and GSSG levels were determined by luminescence-based assay after 24 hour treatment with DMSO or 20 μM DCAC50, and presented as fold-change relative to control, with mean ± SD of three biological replicates. *$P < 0.05$, compared to DMSO control, according to two-tailed Student's *t*-test. **D**. Basal glutathione levels in claudin-low and basal-like cell lines presented as mean ± SD of three biological replicates. **E**. Total SOD activity in cells treated with 20 μM DCAC50 or 30 μM TM, normalized to protein content and presented as the fold-change relative to control, with mean ± SD of at least two biological replicates. **F**. Semi-quantitative SOD1 activity in cells treated with DMSO, 20 μM DCAC50 or 30 μM TM for 24 h and normalized to SOD1 expression. Representative results of two biological replicates (see Supplementary Fig. S4 for examples of full gels and blots).

Figure 5. Effect of DCAC50 on angiogenesis and tumor growth in MDA-MB-468 xenograft mouse model. A. LOX activity proportional to fluorescence intensity measured in media from HuVEC cells incubated with 20 μM DCAC50, 30 μM TM or DMSO for 24 h. Mean ± SD reported for two independent experiments each with three biological replicates. **B**. Representative images of network-formation in HuVEC cells plated on Matrigel membrane matrix with 20 μM DCAC50, 30 μM TM or DMSO for 16 h. Scale bar = 100 μm. **C**. Quantification analysis of angiogenesis features in network-formation assay. Three biological replicates for each treatment were analyzed. Data reported as mean ± SD. *$P < 0.05$, compared to DMSO control, according to unpaired *t*-test. The Holm-Sidak method was used to correct for multiple comparisons in (C). **D**. Tumor volumes in MDA-MB-468 mouse model at the end of treatment. Data are expressed as mean ± SD. *$P < 0.05$, compared to DMSO control, according to two-tailed Student's *t*-test. **E-F**. Effect of DCAC50 on angiogenesis in MDA-MB-468 mouse model. Quantification of (E) $CD31^+$ and (F) $CD31^+CD105^+$ angiogenic blood vessels in the 400 μm tumor macrosections for DMSO and DCAC50 treatment groups. Data are expressed as mean ± SD for three biological replicates. *$P < 0.05$ compared to DMSO control, according to unpaired *t*-test. **G**. Z-stack projections of $CD31^+$ and $CD105^+$ angiogenic blood vessels in a representative macrosection. Scale bars are 500 μm.

Figure 6. Evaluation of DCAC50 in treatment combination with paclitaxel. A. Dose-response profile of single drugs or their combination in MDA-MB-468 cells. Cells were treated with constant ratios of paclitaxel and/or DCAC50 for 72 h. **B**. CI and DRI calculated with CompuSyn Software. CI = [0.9-1.1], additive; CI ≤ 0.90, synergistic. Results of at least three independent experiments are shown. **C**. Oxidative stress in cells treated with paclitaxel, DCAC50 or their combination. TNBC cells were treated for 24 h with DMSO, 10 nM paclitaxel, 20 μM DCAC50, or their combination, and stained with DCFDA. Data are presented as fold-change of DCF fluorescence intensity (mean ± SD of two biological replicates).

Figure 1

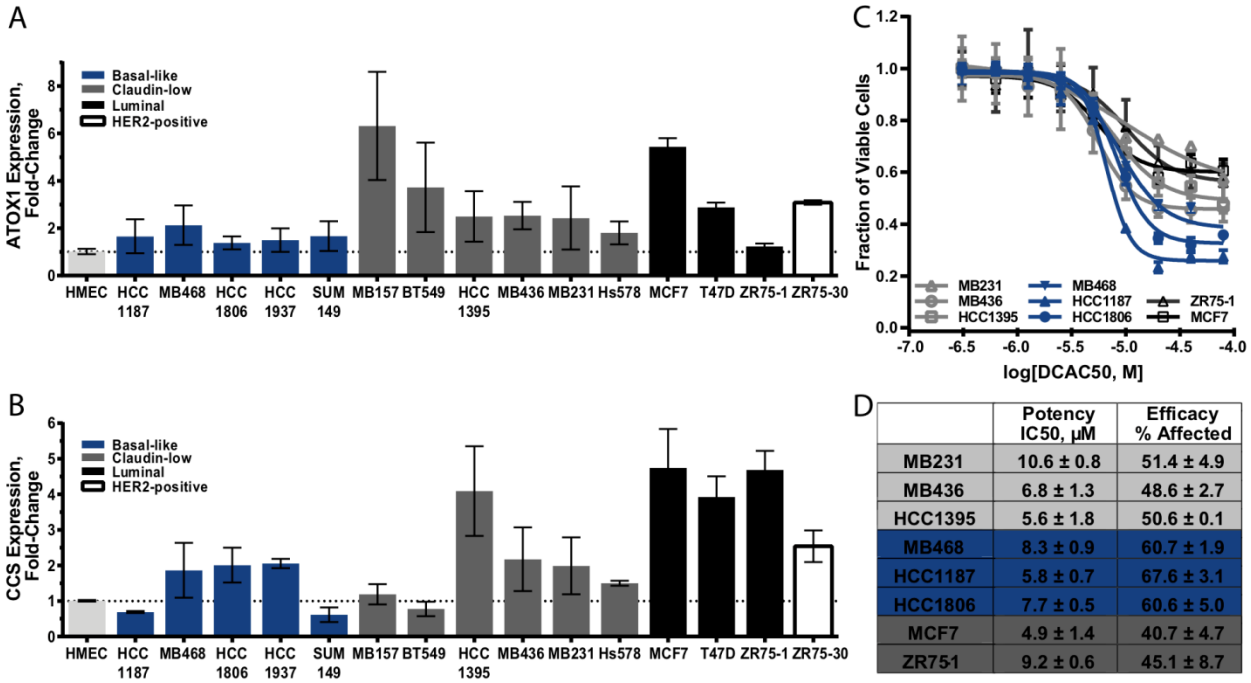

	Potency IC50, µM	Efficacy % Affected
MB231	10.6 ± 0.8	51.4 ± 4.9
MB436	6.8 ± 1.3	48.6 ± 2.7
HCC1395	5.6 ± 1.8	50.6 ± 0.1
MB468	8.3 ± 0.9	60.7 ± 1.9
HCC1187	5.8 ± 0.7	67.6 ± 3.1
HCC1806	7.7 ± 0.5	60.6 ± 5.0
MCF7	4.9 ± 1.4	40.7 ± 4.7
ZR751	9.2 ± 0.6	45.1 ± 8.7

Figure 2

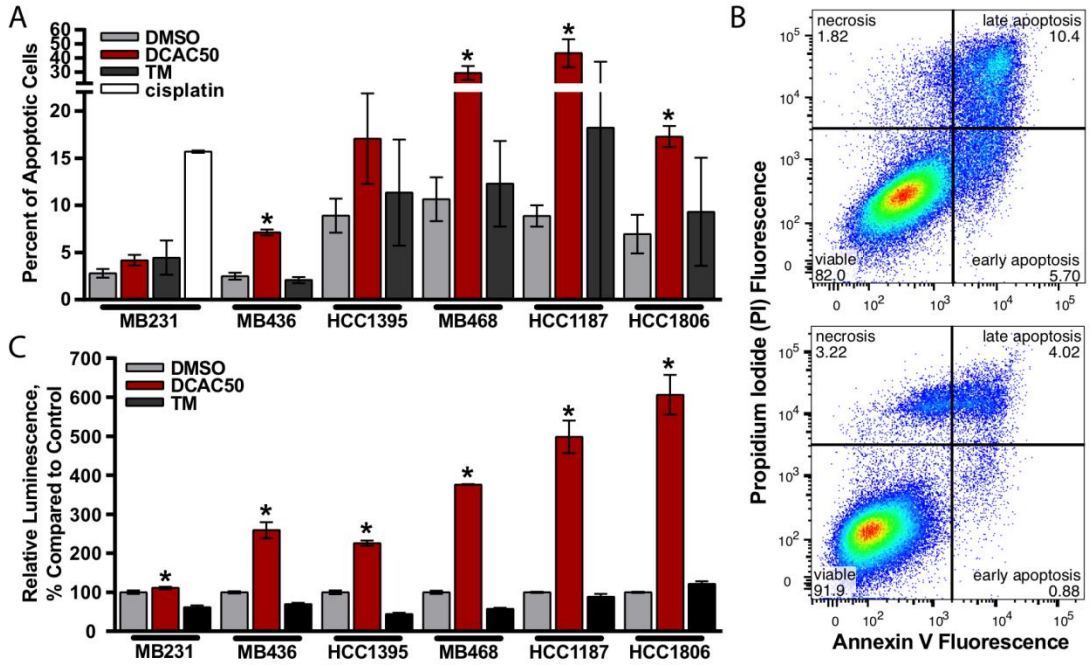
A
Percent of Apoptotic Cells
DMSO
DCAC50
TM
cisplatin
MB231
MB436
HCC1395
MB468
HCC1187
HCC1806
B
necrosis
1.82
late apoptosis
10.4
viable
82.0
early apoptosis
5.70
necrosis
3.22
late apoptosis
4.02
viable
91.9
early apoptosis
0.88
Propidium Iodide (PI) Fluorescence
Annexin V Fluorescence
C
Relative Luminescence, % Compared to Control
DMSO
DCAC50
TM
MB231
MB436
HCC1395
MB468
HCC1187
HCC1806

Figure 3

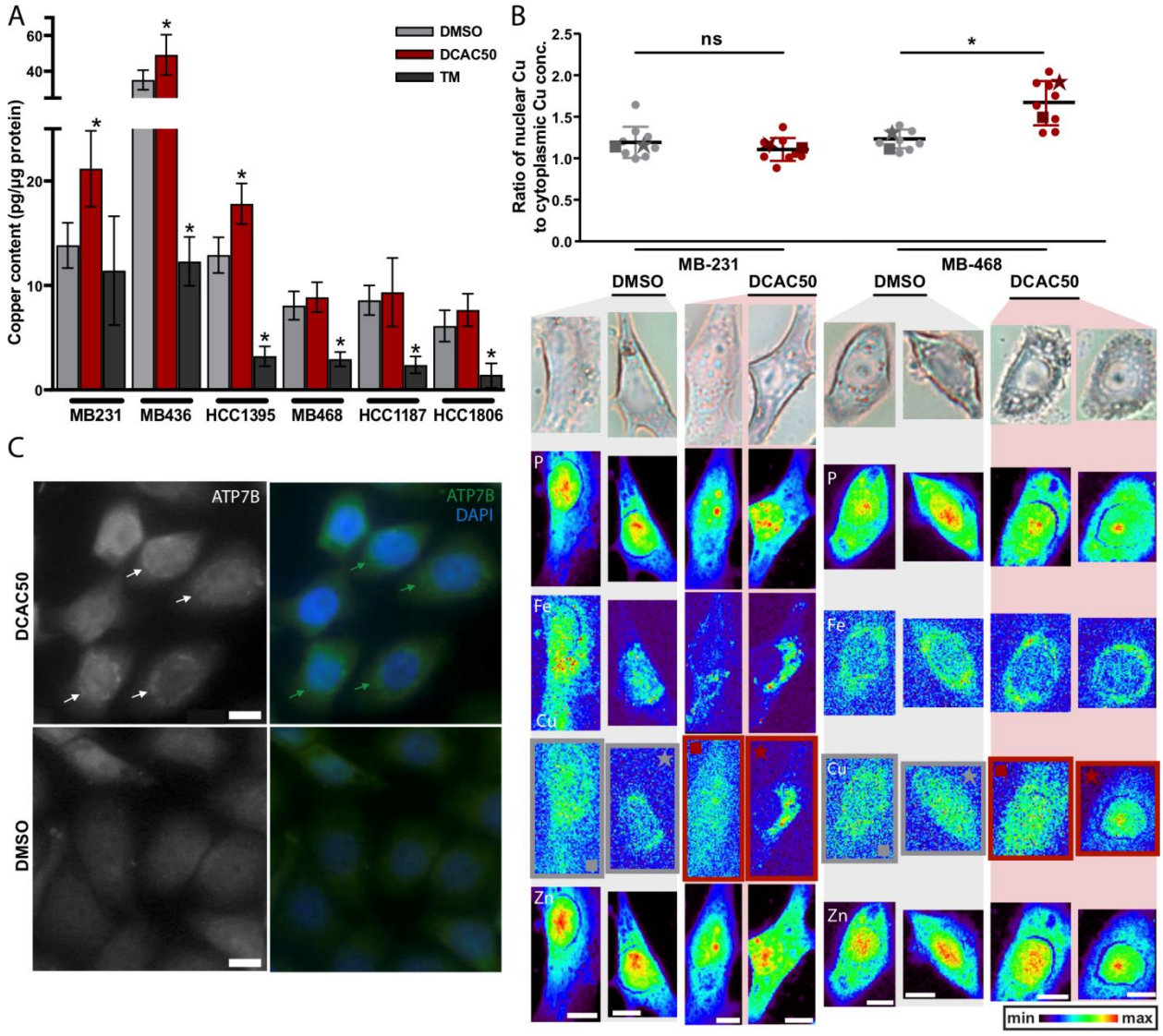
A
DMSO
DCAC50
TM
Copper content (pg/µg protein)
MB231
MB436
HCC1395
MB468
HCC1187
HCC1806
B
Ratio of nuclear Cu to cytoplasmic Cu conc.
ns
*
MB-231
MB-468
DMSO
DCAC50
DMSO
DCAC50
C
ATP7B
ATP7B DAPI
DCAC50
DMSO
P
Fe
Cu
Zn
min
max

Figure 4

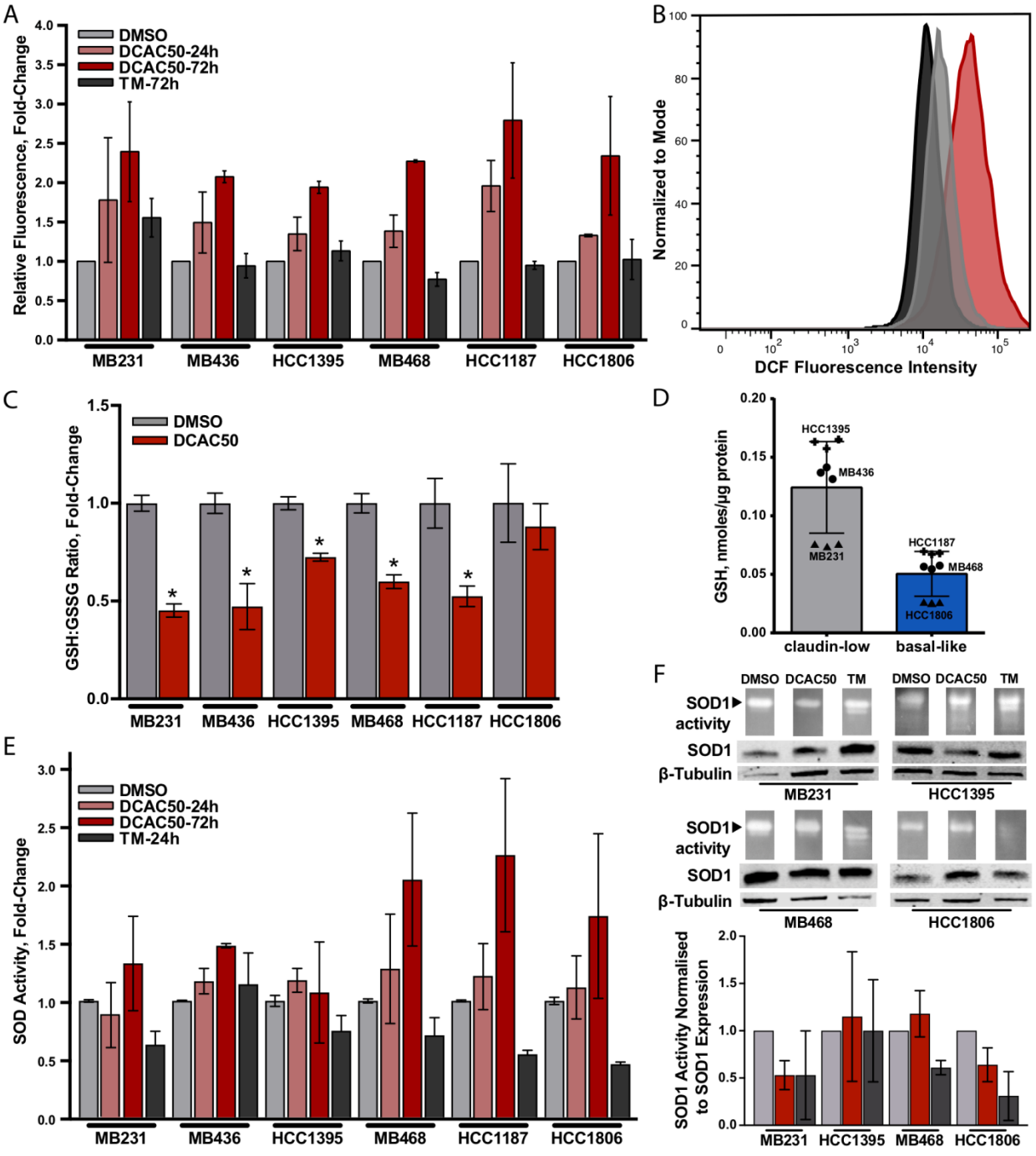
A
Relative Fluorescence, Fold-Change
DMSO
DCAC50-24h
DCAC50-72h
TM-72h
MB231
MB436
HCC1395
MB468
HCC1187
HCC1806
B
Normalized to Mode
DCF Fluorescence Intensity
C
GSH:GSSG Ratio, Fold-Change
DMSO
DCAC50
D
GSH, nmoles/µg protein
HCC1395
MB436
MB231
HCC1187
MB468
HCC1806
claudin-low
basal-like
E
SOD Activity, Fold-Change
DMSO
DCAC50-24h
DCAC50-72h
TM-24h
F
DMSO DCAC50 TM
SOD1 activity
SOD1
β-Tubulin
SOD1 Activity Normalised to SOD1 Expression

Figure 5

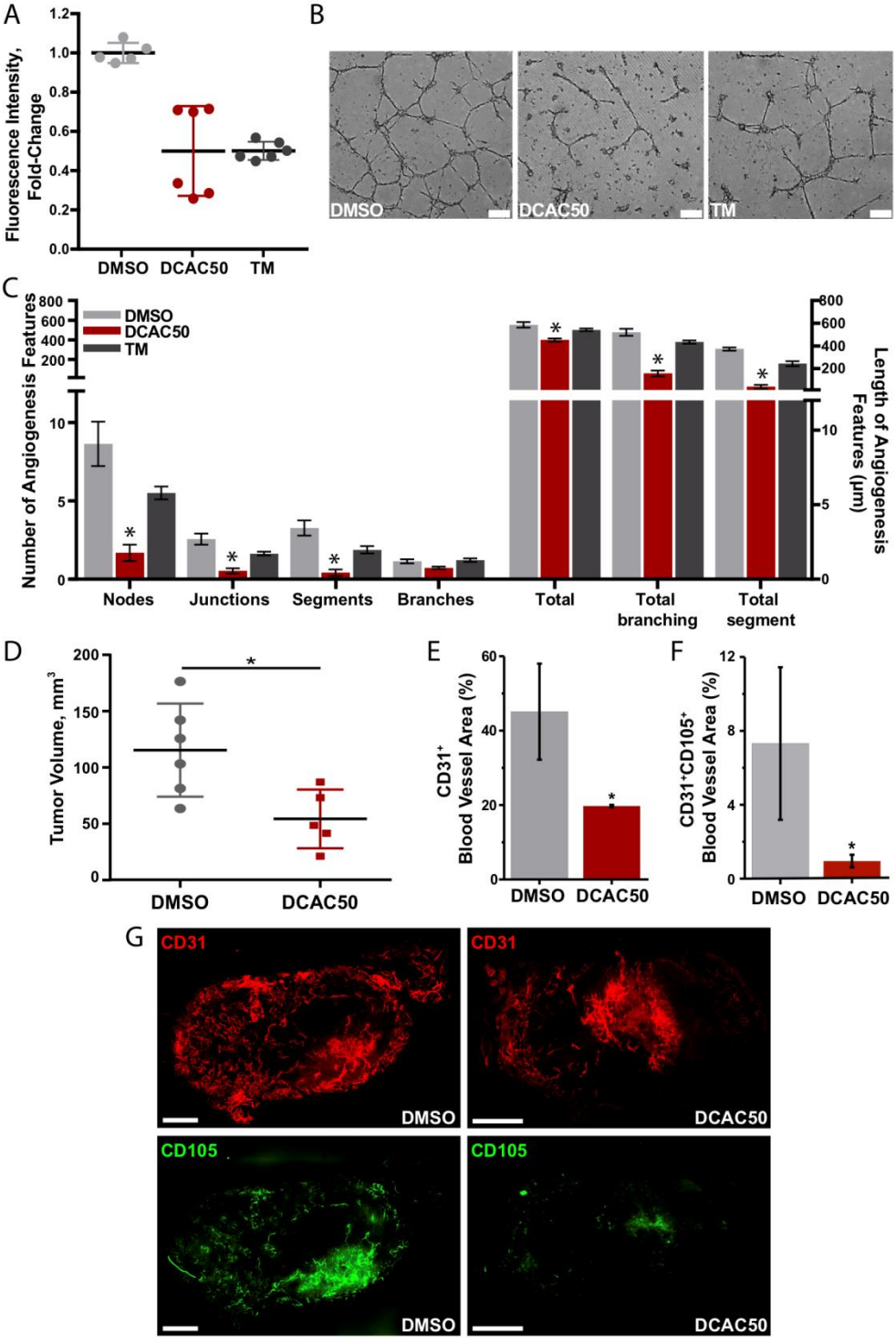
A
Fluorescence Intensity, Fold-Change
1.2
1.0
0.8
0.6
0.4
0.2
0.0
DMSO
DCAC50
TM
B
DMSO
DCAC50
TM
C
Number of Angiogenesis Features
800
600
400
200
10
5
0
DMSO
DCAC50
TM
Length of Angiogenesis Features (μm)
Nodes
Junctions
Segments
Branches
Total
Total branching
Total segment
D
Tumor Volume, mm3
200
150
100
50
0
DMSO
DCAC50
E
CD31+ Blood Vessel Area (%)
60
40
20
0
DMSO
DCAC50
F
CD31+CD105+ Blood Vessel Area (%)
12
8
4
0
DMSO
DCAC50
G
CD31
DMSO
CD31
DCAC50
CD105
DMSO
CD105
DCAC50

Figure 6

A

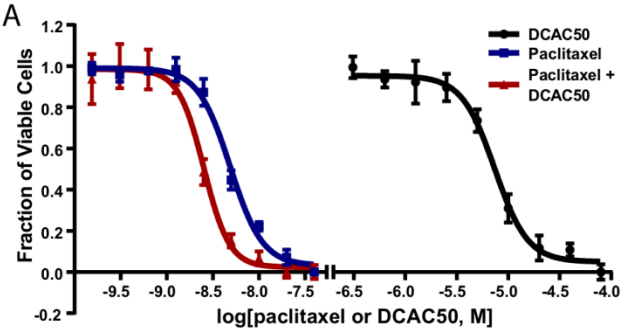

B

	CI	DRI	
	Paclitaxel + DCAC50	DCAC50	Paclitaxel
MB231	0.99	2.10	2.04
MB436	0.95	1.60	3.72
HCC1395	0.89	1.87	3.47
MB468	0.92	2.34	2.15
HCC1187	0.73	2.94	3.14
HCC1806	0.70	3.45	2.74

C

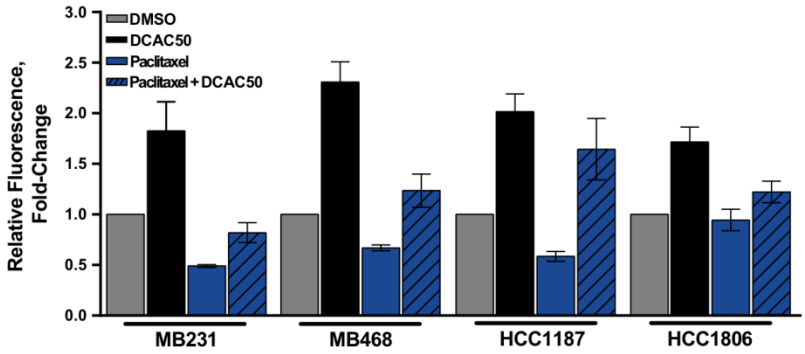

Author/s:
Karginova, O; Weekley, CM; Raoul, A; Alsayed, A; Wu, T; Lee, SS-Y; He, C; Olopade, O

Title:
Inhibition of Copper Transport Induces Apoptosis in Triple-Negative Breast Cancer Cells and Suppresses Tumor Angiogenesis

Date:
2019-05-01

Citation:
Karginova, O., Weekley, C. M., Raoul, A., Alsayed, A., Wu, T., Lee, S. S. -Y., He, C. & Olopade, O. (2019). Inhibition of Copper Transport Induces Apoptosis in Triple-Negative Breast Cancer Cells and Suppresses Tumor Angiogenesis. MOLECULAR CANCER THERAPEUTICS, 18 (5), pp.873-885. https://doi.org/10.1158/1535-7163.MCT-18-0667.